Crystallization Kinetics of Fully Hydrogenated Palm Oil in Sunflower Oil Mixtures

William Kloek[1], Pieter Walstra, and Ton van Vliet*

Wageningen Agricultural University, 6700 EV Wageningen, The Netherlands

ABSTRACT: The crystallization kinetics of mixtures of fully hydrogenated palm oil (HP) in sunflower oil (SF) was studied. The thermal properties and phase behavior of this model system were characterized by means of differential scanning calorimetry and X-ray diffraction. From the melting enthalpy and clear point of HP, it was possible to calculate the supersaturation at a given temperature for every composition of the model system. Supersaturation of the model system for the β′ but not for the α polymorph yielded the β′ polymorph, while supersaturation for the α polymorph yielded a mixture of mainly β and some β′ polymorphs. The crystallization kinetics of HP/SF mixtures were determined by pulsed wide-line proton nuclear magnetic resonance for various initial supersaturations in the β′ polymorph. The determined curves were modeled by a modified classical nucleation model and an empirical crystal growth function, which are both functions of supersaturation. Heterogeneous nucleation rates in the β′ polymorph yielded a surface Gibbs energy for heterogeneous nucleus formation of 3.8 $mJ \cdot m^{-2}$. About 80% of the triglyceride was assumed to be in a suitable conformation for incorporation in a nucleus. Induction times for isothermal crystallization in the β′ polymorph yielded a surface free energy for heterogeneous nucleus formation of 3.4 to 3.9 $mJ \cdot m^{-2}$.

Paper no. J9222, *JAOCS 77*, 389–398 (April 2000).

KEY WORDS: Crystal growth, crystallization, fats, kinetics, heterogeneous nucleation, phase behavior, polymorphism, triglycerides.

Fats are being crystallized for various reasons, such as fractionation into certain groups of triglycerides or to give food products a certain texture. For fractionation of groups of triglycerides, it is desirable that the remaining oil can be readily removed from the crystals by washing procedures. Therefore, a small specific crystal surface area, i.e., a large crystal size, is desired. If fats are crystallized to give food products textural properties like spreadability, very small crystals are generally desired. These small crystals aggregate due to van der Waals forces, resulting in large aggregates or a continuous crystal network that gives the dispersions its consistency (1,2). A key parameter for describing the mechanical properties of a fat dispersion is the proportion of crystallized fat. Low solid-fat contents can give a spreadable product, but may also lead to undesired oiling-off, while high amounts of solid fat can give a hard, brittle product (3). Besides by the amount of solid fat, the textural properties will be influenced by crystallization temperature. For example, if a solution of 10% hardened palm oil in sunflower oil has crystallized at 25°C, a spreadable, solid-like dispersion with small crystals is obtained. If the same solution is crystallized at about 38°C it yields at room temperature a dispersion with the same solid-fat content with large spherulitic crystal agglomerates that can be poured at room temperature. The variation in structural properties initially arises from variation in crystal-size distribution and in the arrangement of the crystals in space. Both size and aggregation of the crystals depend on the crystallization kinetics.

A substance can only crystallize if it is supersaturated. A solution is supersaturated if the activity of a dissolved component x is higher than the activity of a saturated solution, i.e., a solution in which crystals and solute are in thermodynamic equilibrium. We then have a chemical potential difference $\Delta\mu$ between the supersaturated and the crystalline material. This $\Delta\mu$ is supposed to be equal to that of a saturated solution. For an ideal solution, the chemical potential difference is given by:

$$\Delta\mu = R_g T \ln \frac{c_x}{x_x} \qquad [1]$$

where R_g is the gas constant, T the absolute temperature, c_x the fraction in solution at supersaturation, and x_x the fraction soluble at saturation. The ratio c_x/x_x is called the supersaturation ratio β, and ln β is the supersaturation. The soluble fraction is given for ideal solutions by the Hildebrand equation (4,5):

$$\ln x_x = \frac{\Delta H_{f,i}}{R_g} \cdot \left(\frac{1}{T_{m,i}} - \frac{1}{T} \right) \qquad [2]$$

where $\Delta H_{f,i}$ is the enthalpy of fusion, and $T_{m,i}$ the melting temperature of pure x in polymorph i. The most common way to supersaturate a solution or to supercool a melt is by decreasing the temperature so that the soluble fraction becomes smaller than the fraction present.

Nucleation. Primary crystallization can be divided into two consecutive processes, nucleation and crystal growth, whose

[1]Address: DMV-International, P.O. Box 13, 5460 BA. Veghel, The Netherlands.

*To whom correspondence should be addressed at Wageningen Agricultural University, Dept. of Food Science, Food Physics Group, P.O. Box 8129, 6700 EV Wageningen, The Netherlands.
E-mail: Ton.vanVliet@phys.fdsci.wan.nl

Copyright © 2000 by AOCS Press

rates both depend on supersaturation. A nucleus is a molecular aggregate of crystalline structure that is large enough for further growth to lead to a decrease of its Gibbs energy. The activation free energy for formation of a spherical nucleus according to classical nucleation theory is given by:

$$\Delta G^*_{3D,\text{hom}} = \frac{16\pi \cdot v_c^2 \cdot \gamma^3 \cdot N_{av}^2}{3 \cdot \Delta\mu^2} = \frac{16\pi \cdot v_c^2 \cdot \gamma^3}{3 \cdot (k_b T)^2 \cdot (\ln\beta)^2} \quad [3]$$

where k_b is Boltzmann's constant, γ is the surface free energy of the nucleus with respect to the mother phase, v_c the molecular volume in a crystal lattice, and N_{av} Avogadro's number. The product $v_c \cdot N_{av}$ equals the molar volume of the substance in a crystal lattice. More precisely, the activation free energy is a Gibbs energy because the pressure is presumably constant. From isothermal crystallization experiments on emulsified hydrogenated palm oil (HP)/sunflower oil (SF) mixtures, we were able to reach conditions of homogeneous nucleation and obtained $\gamma \approx 4.1$ mJ $\cdot$ m^{-2} (6,7). The number of nuclei formed per unit volume and unit time is called the nucleation rate J and is mostly expressed as an Eyring-type equation with ΔG^*_{3D} as the activation free energy for nucleus formation:

$$J = N \cdot \frac{k_b T}{h} \cdot \exp\left(\frac{-\alpha \cdot \Delta S}{R_g}\right) \cdot \exp\left(\frac{-\Delta G^*_{3D}}{k_b T}\right) \quad [4]$$

In this equation, N is the number of crystallizing molecules per unit volume, $k_b T/h$ the natural frequency, where h is Planck's constant, α the fraction of the molecule that should be in the "correct" conformation for incorporation in a nucleus, and $\Delta S = \Delta H_{f,i}/T_{m,i}$ the decrease of entropy on crystallization of one mole of triglyceride. The term $\exp(-\alpha \cdot \Delta S/R_g)$ is proportional to the probability that a triglyceride molecule at the crystal surface is in the right conformation for incorporation in a nucleus. Skoda and van den Tempel suggested that the growth of triglyceride molecules is mainly determined by the probability that the long fatty acid chains are in a suitable conformation (8). For this type of molecule, this will be mainly determined by the loss of entropy. It is likely that the same loss of entropy can also delay nucleation (Wouter Meeussen, personal communication). To our knowledge, such an approach in fat crystallization is never applied. From homogeneous nucleation rates in the α polymorph in emulsified HP/SF mixtures, we found that almost the whole molecule had to be in the right conformation for incorporation in an embryo/nucleus (6,7). In bulk fats, nucleation is heterogeneous, which can be expressed by a smaller ΔG^*_{3D} due to a smaller nucleus size or a smaller effective γ.

Crystal growth. The growth kinetics describes the crystal growth rate of a crystal face as function of supersaturation or supercooling. For detailed discussions on crystal growth, see some review papers (9–11). The growth rate of a crystal face depends on the state of the crystal surface, or more precisely, on the strength of the bonds in the connected network in the crystal for that face. The state of a surface is defined by the surface entropy factor α_s. At high supersaturation, crystal faces are rough and continuous crystal growth occurs. The growth rate R_c would be proportional to the supersaturation:

$$R_c = A_1 \cdot \ln\beta \quad [5]$$

where A_1 is a constant. At lower supersaturation, two-dimensional nucleation on a flat surface would be necessary for growth of a new crystal layer. This surface nucleation step then is rate-limiting. If a crystal growth is by a surface nucleation process, the growth rate would be given by:

$$R_c = A_1 \cdot (\ln\beta)^p \cdot \exp\left(\frac{A_2}{\ln\beta}\right), \quad \text{with} \frac{-3}{2} \le p \le \frac{5}{6} \quad [6]$$

The constant A_2 contains the activation free energy for formation of a surface nucleus of critical size.

At low supersaturation, the activation free energy for surface nucleation can become so high that the crystal surface needs to contain defects, such as screw dislocations, to which growth units can attach. For this type of growth, Burton *et al.* (12) developed the BCF relation (Burton-Cabrera-Franks) that describes the growth rate as a function of the supersaturation:

$$R_c = A_1 \cdot \frac{(\ln\beta)^2}{\ln\beta_c} \cdot \tanh\frac{\ln\beta_c}{\ln\beta} \quad [7]$$

in which $\ln\beta_c$ is a constant specific to the system.

Only few accurate crystal growth rate measurements on triglycerides can be found in the literature. Skoda and van den Tempel determined growth rates of the lateral faces of single tristearate crystals in tristearate/trioleate mixtures at low supersaturations (8). For $\ln\beta < 0.47$, the crystals became regularly shaped, and the growth rate increased nonlinearly with $\ln\beta$. According to the authors, growth by a surface nucleation mechanism could be ruled out because of the nonlinearity of a plot of the logarithm of the growth rate against the reciprocal supersaturation. For $\ln\beta > 0.47$, the crystals were irregularly shaped, and the growth rate increased about linearly with $\ln\beta$. Skoda and van den Tempel stated that due to the presence of permanent steps of about 4 Å, the short spacing length of triglycerides, no surface nucleation is necessary for growth (8). Steps with a height of about 4.5 Å were shown in electron micrographs of triacylglycerol crystals (13). The presence of permanent steps would lead to continuous growth, and Skoda and van den Tempel suggested that the growth rate then is mainly determined by the probability that the triglycerides have a suitable orientation for incorporation in the surface (8). Other triglycerides, such as tripalmitin and glycerol, 1,3-dipalmitate-2-stearate (PPP and PSP, respectively), showed similar growth behavior.

Another important observation was that the growth rate at a certain $\ln\beta$ was history-dependent. If a crystal was first grown at a certain supersaturation and subsequently grown at a lower one, the growth rate at this low supersaturation was slower than if this lower supersaturation had directly been applied. This implies that the state of the crystal surface, and thereby crystal growth, can be influenced by the growth history. This observation can have important consequences for the crystal growth

rate of natural fats because they contain hundreds of different triglycerides.

The aim of this work is to describe the crystallization kinetics of the model fat dispersion in terms of nucleation rates and crystal growth rates. To this end, also the polymorphic behavior of this model system is studied.

EXPERIMENTAL PROCEDURES

Materials. The model system consisted of mixtures of HP and SF, the HP providing the solid phase and the SF the liquid phase. None of the fats was purified. Fatty acid compositions and the distribution over 1,2 and 3 positions of the glycerol molecule are discussed in another paper (7). The main triglycerides were glycerol, 1-palmitate-2,3-distearate (PSS; 26%) and PSP (39%). The HP contains less than 1% monoglycerides, about 6% diglycerides, and about 94% triglycerides. The average molar masses of HP and SF were calculated from the fatty acid compositions and were 854 and 877 g/mol, respectively. The melting temperatures of HP in the α and β′ polymorphs are 41.8 and 57.3°C, respectively. The molar melting enthalpies of HP in the α and β′ polymorphs are 98 and 161 kJ/mol. These data will be discussed in the Results and Discussion section. They will be used to calculate the supersaturation (ln β) of a HP/SF mixture at a certain temperature or to calculate the desired crystallization temperature to have an HP/SF dispersion crystallized at a certain initial supersaturation by using Equation 1 and Equation 2.

Methods. Mixtures of HP in SF were made by melting the HP at 80°C and bringing an amount of liquid HP in a vessel. Care was taken that the HP remained liquid while transferring it to the vessel, thus avoiding fractionation due to crystallization. An appropriate amount of SF was added to give the final mixture. Prior to every experiment, the mixtures were kept at 80°C for 10 min to destroy any crystal memory.

The melting and crystallization behaviors of HP/SF mixtures were studied by means of differential scanning calorimetry (DSC) with a Mettler DSC-30, equipped with a TC-10A processor or a TA-Instruments DSC-type 2910. The α polymorph was obtained by cooling the HP/SF mixture from 80 to –40°C at a rate of 20 K/min while measuring the heat flow. The peak temperatures as function of fraction HP were used to obtain the enthalpy of fusion and the crystallization temperature of the α polymorph of HP by fitting them to the Hildebrand equation. After crystallization in the α polymorph, the mixtures were heated at a rate of 2 K/min from –40 to 80°C while measuring the heat flow. This heating scan yielded, dependent on the fraction HP, a recrystallization peak from α to the β polymorph and the melting endotherm of the β polymorph. The peak temperature of this β melting peak as function of the fraction HP was used to calculate the melting enthalpy and the melting temperature of the β polymorph of HP by fitting them to the Hildebrand equation. To obtain the β′ polymorph, the HP/SF mixture was cooled at a rate of 10 K/min from 80°C to 4 K above the α clear point of that dispersion and allowed to crystallize isothermally for 30 min. After isothermal crystallization, the sample was cooled to –5°C and then heated at a rate of 2 K/min to 80°C while recording the β′ melting endotherm. The α clear point was calculated from the Hildebrand equation by inserting the appropriate fraction HP (x_{HP}), a molar melting enthalpy of 98 kJ/mol, and a melting temperature of 315 K (41.8°C). The latter two were determined by fitting the α crystallization exotherm peak temperatures to the Hildebrand equation (see Results and Discussion section).

Time-resolved X-ray diffraction was used to determine the short spacings, from which the crystal polymorph can be extracted. The radiation source used (Cu-$K_{\alpha 1}$) operated at a wavelength of 1.5405 Å. Radiation was detected by using an 1025-channel digital diode array positional detector. The position of the detector was calibrated with potassium iodide (4.08 and 3.53 Å). The sample holder could be heated and cooled at rates of about 1 K/s. The α polymorph of pure HP was obtained by cooling the sample from 80 to 5°C at an approximate rate of 1 K/s. The β′ polymorph was obtained by cooling the sample from 80 to 45°C at the rate of 1 K/s and allowing the sample to crystallize isothermally for 30 min. X-ray spectra were recorded every 5 s.

Isothermal crystallization of HP/SF mixtures was monitored by pulsed wide-line proton nuclear magnetic resonance spectroscopy (p-NMR) with a Bruker minispec P20i (Karlsruhe, Germany). The HP/SF mixture, which was placed in an NMR tube, was first kept at 80°C for 10 min and then placed in a waterbath that was at the desired temperature. The time needed to obtain the desired temperature was about 20 s. The amount of solid fat was determined by measuring the relaxed signal twice after applying a 90° pulse. The signal could not be measured during the first 10 μs after the pulse was applied due to electronic recovery from the electromagnetic pulse. Within this time, a part of the signal from protons in the crystal lattice had already decayed. After 40 μs, the signal from the solid protons decayed, and the signal was due only to the signal of the liquid protons. The measured signal was proportional to the amount of protons. From the measured signals at 10 and 90 μs after applying a 90° pulse, and after applying a correction for the signal decay between 0 and 10 μs after the pulse by means of an *f*-factor, the fraction solid can be calculated. The *f*-factors were determined from the measured NMR signals and the expected fractions solids from Equation 2 by using values of $\Delta H_{f,i}$ and $T_{m,i}$ that were determined by DSC. The *f*-factors for HP/SF mixtures crystallized in the α and β′ polymorph were 1.14 and 1.44, respectively. The solid fat fraction was determined by averaging the signals from three pulses at repetition times of 5 s. This repetition time was sufficient to avoid saturation of the signal due to incomplete relaxation. The reproducibility of this determination was about 0.3–0.4 % solid fat.

RESULTS AND DISCUSSION

Thermal properties of HP. Figure 1 shows the thermal effects during heating of HP that had crystallized at various conditions. The samples were first quenched to –80°C to crystallize the HP. During heating of the sample (trace 1) at a rate of 2

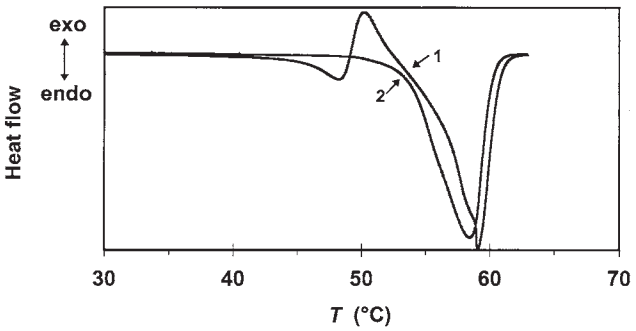

FIG. 1. Differential scanning calorimetry (DSC) heating curves of hydrogenated palm oil (HP), crystallized by rapid cooling from –80 to 80°C. Trace 1: heating from –80 to 80°C at 2 K·min^{-1}. Trace 2: heating from 5 to 80°C at 2 K·min^{-1} after isothermal crystallization for 30 min at 50 and cooling to 5°C (graph only shows traces starting at 30°C).

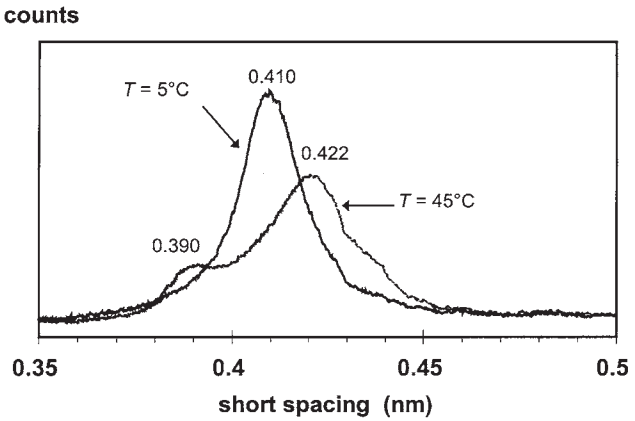

FIG. 2. X-ray diffraction spectra of HP crystallized at 5 and 45°C. The indicated numbers are the spacings in nm. Characteristic short spacings are (Ref. 14): α, 0.415 (s)/β′, 0.38(s) and 0.42(s)/β, 0.46 and 0.36–0.39 nm; (s) = strong. See Figure 1 for abbreviation.

K/min, first an endothermic peak was observed, followed by an exothermic peak, and finally a large endothermic peak. As the HP was cooled rapidly to –80°C, it is likely that at least part of the HP had crystallized in the most unstable α polymorph. The first endotherm on heating (T = 48°C) then would correspond with melting of the α polymorph, and the exotherm at 50°C with recrystallization of the α polymorph to a more stable polymorph (β′ and/or β). The final endotherm around 59°C would correspond with melting of the more stable polymorph. Simultaneous with endothermal melting of the α polymorph, some exothermal recrystallization to a more stable polymorph may have occurred, which might explain the small melting endotherm of the α polymorph as compared to the large melting endotherm of the more stable polymorph. The final endotherm seems to be formed by more than one peak, which suggests the simultaneous occurrence of different polymorphs, or the existence of compound crystals, or both.

When the melting scan was stopped at 50°C for 30 min to allow HP to (re)crystallize isothermally, followed by cooling to 5°C and then determining a melting scan (trace 2), only an endothermic melting effect was observed. The peak temperature was at a lower temperature than in a continuous scan, and the melting peak seemed to be smooth. This indicates that, after isothermal crystallization at a temperature slightly above the α melting temperature, HP crystallizes in a less stable polymorph, probably the β′ polymorph. The width of the melting peak (more than 10 K) suggests that a range of compound crystals of different composition melt.

The polymorphic forms were checked by determining X-ray diffraction spectra for HP, crystallized at 5 and 45°C for 30 min (Fig. 2). It is clear that isothermal crystallization at 5°C predominantly yielded the α polymorph, while crystallization at 45°C almost exclusively yielded the β′ polymorph. It is not clear whether heating of HP that had crystallized in the α polymorph yielded the β′ polymorph, the β polymorph, or a mixture of both. The latter seems the most likely. In the absence of oil and at room temperature, the α polymorph was observed to be stable for at least 30 min.

Thermal properties of HP/SF mixtures. The DSC melting curve of HP in the β′ polymorph only shows one broad melting peak (Fig. 1; trace 2). Although extensive compound crystal formation will occur owing to the variety of triglycerides present, we will treat HP as a one-component system with one melting point and one melting enthalpy for each polymorph. This is allowed because the triglycerides in HP are all similar: They all contain completely saturated fatty acid residues and most of these are palmitic and stearic acid. We will also treat the SF as a one-component system. Under the experimental conditions, SF will always be liquid. Because the melting points of HP and SF differ by more than 45 K, the solubility of HP in SF can be approximated by the Hildebrand equation (Eq. 2) (4,5). This equation assumes ideal mixing behavior, which will not be quite true for the β′ polymorph in our system. By fitting the melting temperatures of a certain polymorph of mixtures that contain various amounts of HP to the Hildebrand equation, effects due to nonideal mixing will be incorporated in the calculated melting enthalpy and melting temperature. However, the combination of the experimental values of melting enthalpy and melting temperature would provide an almost correct solubility of HP in SF.

The α polymorph can be obtained by cooling a solution so rapidly that nucleation in the β′ or β polymorph does not occur. Because the α polymorph in bulk fats cannot be supercooled deeply, the onset temperature or the peak temperature measured by DSC would only be a little below the α clear point. After crystallization in the α polymorph, the mixtures were heated. On heating, none of the HP/SF mixtures showed an α-melting peak; nevertheless, an exothermal crystallization peak was present. The endothermal effect of melting of the α polymorph may have been masked by the simultaneous exothermal effect of recrystallization in the more stable polymorph. Melting of the recrystallization product showed a large endothermic melting peak (β′ and/or β polymorph). This peak did not show a discontinuity, as seen for a 100% HP sample. To obtain the β′ polymorph, solutions were kept for 30 min at a temperature 4 K above the clear point of α crystals. After cooling back

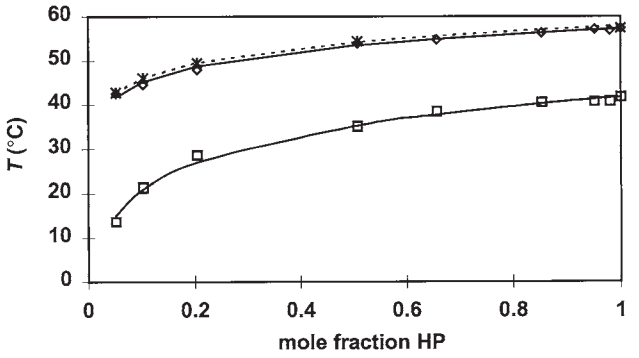

FIG. 3. Peak temperatures of the crystallization and melting processes measured by DSC as function of the fraction HP in HP/sunflower oil (SF) mixtures. □, crystallized in the α polymorph; ◇, melting after crystallization in the α polymorph (which obtained the β polymorph); *, melting after isothermal crystallization at 4 K above the α clear point (which obtained the β′ polymorph). The lines were fitted to the Hildebrand equation. See Figure 1 for abbreviations.

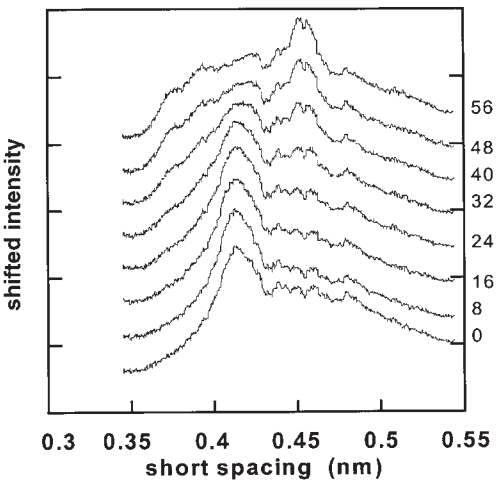

FIG. 4. X-ray diffraction spectra (short spacings) of a 10% HP/SF mixture crystallized at 5°C as function of holding time (indicated in minutes near right-hand *y*-axis). See Figure 1 and 2 for abbreviations.

to −5°C, the DSC melting profile was measured. Figure 3 shows that the measured peak temperatures can be fitted well with the Hildebrand equation, yielding the molar melting enthalpy and the melting temperature of HP. The figure shows hardly any difference between melting of the polymorph obtained after melting of the α polymorph (which consists mainly of the β polymorph) and the polymorph obtained after isothermal crystallization at 4 K above the α clear point (which is the β′ polymorph).

The melting enthalpies and melting temperatures obtained from the fit of the thermal data of HP/SF mixtures, together with the data for 100% HP, are given in Table 1 and will be compared with each other. The fitted melting temperatures correspond well with the temperatures measured for pure HP for all polymorphs. There is only a slight difference in the enthalpy of fusion for the α polymorph obtained from HP (98 kJ/mol) and from the mixtures (84 ± 0.8 kJ/mol), which suggests that the Hildebrand equation well describes the solubility of the α polymorph of HP in SF. Wesdorp concluded from an extensive study that the formation of compound crystals in the a polymorph hardly disturbed crystal packing due to freedom of the fatty acid chain for oscillations (5). Therefore, the mixing of the solid phase in the α polymorph is about ideal.

There was a considerable difference between the melting enthalpy for HP obtained from the fit of the peak temperatures and that obtained from the pure HP sample when crystallization occurred in a more stable polymorph (β′ or β). This is probably due to nonideal mixing behavior in the β′ and β polymorphs and compound crystal formation (5). Another possibility for the lower molar enthalpy of "pure" HP is that liquid impurities present in HP are dissolved in the oil phase of HP/SF mixtures and therefore do not cause defects in HP crystals formed. There is no significant difference between the melting temperatures, when the more stable polymorph is prepared by recrystallization from the α polymorph (57.2 ± 0.5°C) or by direct crystallization at a temperature above the α clear point (57.3 ± 0.7°C).

Although melting temperatures and melting enthalpies obtained from DSC melting scans can give some indication about the polymorph(s) present, the only reliable way to determine this is by means of X-ray diffraction. Therefore, we determined X-ray spectra of 10% HP/SF mixtures that had isothermally crystallized at 5 and 15°C. Figure 4 clearly shows that, at a temperature of 5°C, crystallization takes place in the α polymorph (short spacing 0.415 nm). The intensity of the α peak at

TABLE 1
Melting Enthalpies and Melting Temperatures of Hydrogenated Palm Oil[a]

Experiment (polymorph indicated)	From mixtures $\Delta H_{f,i}$ (J·mol^{-1})	From mixtures $T_{m,i}$ (°C)	From pure HP $\Delta H_{f,i}$ (J·mol^{-1})	From pure HP $T_{m,i}$ (°C)
α-Crystallization exotherm (α)	(8.4 ± 0.8)·10^4	41.9 ± 1	9.8·10^4	41.8
Melting after α-crystallization endotherm (β)	(1.7 ± 0.1)·10^5	57.2 ± 0.5	1.12·10^5	57.4
Melting after β′-crystallization endotherm (β′)	(1.6 ± 0.1)·10^5	57.3 ± 0.7	1.35·10^5	57.6

[a]Enthalpies and melting temperatures with 95% confidence limits obtained by fitting peak transition temperatures of hydrogenated palm oil/sunflower oil(HP/SF) mixtures to the mole fraction of HP by using the Hildebrand equation.

0.415 nm decreased in time, and peaks at 0.37 and 0.39 nm and a strong double peak at 0.45–0.46 nm appeared or increased in intensity. These peaks correspond to the β polymorph (14). There is also an increase in intensity of a peak at 0.42 nm, which corresponds to the β′ polymorph. Crystallization in the α polymorph of HP/SF mixtures thus leads to a fast transformation to a mixture of some β′ crystals and predominantly β crystals.

At 5°C the polymorphic transformation from α to β′/β in a 10% HP/SF mixture took about 30 min. Isothermal crystallization experiments at 15°C showed a transformation in about 3 min. Pure HP, crystallized at 5°C, did not show any transformation at this temperature in 30 min. This shows that both the presence of a liquid phase and higher temperatures enhance transformation from the α polymorph to a more stable one.

The activation energy for the polymorphic transition can be estimated from the time scales of the transition at the two temperatures. The time scales of the transitions are inversely proportional to the reaction rate of the transitions. The reaction rate is, in turn, proportional to $\exp[-\Delta E^*_a/(R_g T)]$, where ΔE^*_a is the activation energy of the rate-limiting step of the polymorphic transition. The ratio between the time scales of the transition at temperatures T_1 and T_2 is given by $\exp[-\Delta E^*_a/R_g \cdot (T_1^{-1} - T_2^{-1})]$, from which ΔE^*_a can be calculated. Substituting time scales of 1,800 and 180 s at temperatures of 278 and 288 K, respectively, would give an activation energy of 153 kJ·mol^{-1}. This value is close to the melting enthalpy of HP in the β′/β polymorph, as determined from the melting curves of HP/SF mixtures. Therefore, it is likely that crystallization of the β′/β polymorph is the rate-limiting step in the polymorphic transition of the α polymorph. Probably the transition occurs by a dissolution–crystallization process because it is associated with a change in the extent of compound crystal formation. Initiation of the more stable polymorph can occur by nucleation in this polymorph, because the solubility of the α polymorph in the SF is small at the prevailing conditions, so that the soluble material can become supersaturated for the more stable polymorph. The solubilities of the α polymorph at temperatures of 5 and 15°C are, according to the Hildebrand equation, 0.7 and 3%, respectively. The solubilities of the β′ polymorph at these temperatures are 0.00164 and 0.0184%, respectively. At these conditions, ln β of the dissolved triglycerides in the β′ polymorph, assuming their thermodynamic properties to be the same as for HP, would equal ln(0.7/0.00164) = 6.1 and ln(3/0.0184) = 5.1, respectively.

If the mixtures had crystallized at a temperature above the onset of the α-clear point, X-ray diffraction spectra only showed the β′ polymorph, even after several days of storage. This leaves the question as to why the transformation α → (β′, β) does occur, even with some preference for the β polymorph, while after crystallizing in the β′ polymorph, no transition to the β polymorph occurs. This is probably due to the formation of compound crystals. Extensive compound crystal formation in the α polymorph will lead to a large difference in chemical potential difference between the α polymorph and the most stable β polymorph, and thereby to a considerable driving force for recrystallization. Formation of compound crystals in the β′ polymorph is less extensive, and the driving force for recrystallization would thus be smaller.

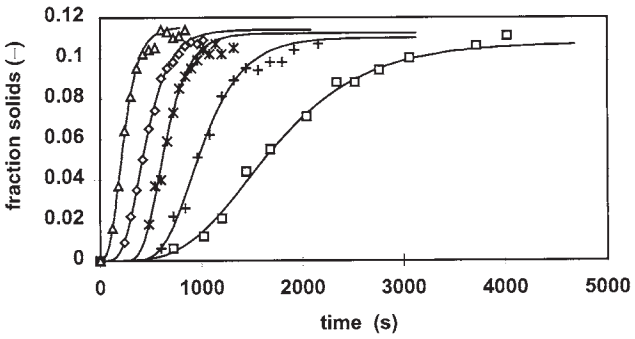

FIG. 5. Isothermal crystallization curves of 12% HP/SF mixtures at various initial supersaturations. Solid lines are fitted with the Gompertz equation. Supersaturation (*T* in °C): □, 2.25 (34.5), + 2.50 (33.3); *, 2.75 (32.1); ◇, 3.00 (30.9); △, 3.25 (29.7). See Figures 1 and 3 for abbreviations.

Crystallization kinetics. The crystallization kinetics of mixtures, containing 6, 8, 10, 12, or 14% HP/SF, at initial supersaturations in the β′ polymorph ranging from 2.25 to 4.00 in steps of 0.25, were determined by p-NMR. This means that for each HP/SF mixture and initial supersaturation, a different crystallization temperature was used. For a 10% HP/SF mixture, the crystallization temperatures for an initial supersaturation of 2.25 and 4.00 were 33.5 and 25.3°C, respectively, while for the 14% HP/SF mixture, they were 35.3 and 26.2°C, respectively. These different temperatures at the same initial ln β will also lead to differences in continuous phase viscosity, which will certainly influence mass transport of molecules from the bulk to the crystal surface.

Figure 5 shows the determined crystallization curves of 12% HP/SF mixtures at various initial ln β. It is clear that the induction time for crystallization increased with decreasing initial supersaturation. This can be explained by the strong dependence of the nucleation rate on supersaturation, according to Equations 3 and 4. The final fraction of solid fat increased with increasing initial supersaturation due to the decrease of solubility, as expected from Equation 2.

To model crystallization kinetics, one has to know the relation between crystal growth rate and supersaturation. To obtain the supersaturation as function of time, we fitted the crystallization curves to a modified Gompertz equation (15). This fit yields an analytical expression that gives the supersaturation as a function of time. A reparameterized Gompertz equation is:

$$s(t) = s_{\max} \cdot \exp\left\{-\exp\left[\frac{\mu \cdot e}{S_{\max}} \cdot (\lambda - t) + 1\right]\right\} \qquad [8]$$

where $s(t)$ is the fraction solid fat at time t and $s_{\max}$ the maximum fraction of solid fat, μ the maximum increase rate in frac-

tion solid fat (or the tangent of the crystallization curve in its inflection point), λ a nominal induction time defined as the intercept of the tangent line at the inflection point with the time-axis, and *e* equals 2.7183. At $t = \lambda$, the fraction solid fat would equal 0.066 s_{max}. The maximum fraction of solid fat s_{max} can be written as:

$$S_{\max} = c_{0,HP} - x_{HP} = c_{0,HP} \cdot \left(1 - \frac{1}{\beta_0}\right) \quad [9]$$

where $c_{0,HP}$ is the fraction HP present and β_0 the supersaturation ratio at the start of crystallization, which are constants. So, only parameters μ and λ are left to fit the crystallization curve. Figure 5 shows that the reparameterized Gompertz equation fitted the crystallization curves well.

The obtained induction time λ can be used to estimate the surface free energy for formation of a nucleus of critical size. If it is assumed that λ is a measure of the nucleation rate in which $\lambda \propto J^{-1}$, we obtain for a nucleus (10):

$$\ln\lambda \propto \frac{\nu_c^{\,2} \cdot \gamma^{-3}}{(k_b T)^3} \cdot \frac{1}{(\ln\beta_0)^2} \quad [10]$$

This equation assumes the collision frequency, and the entropy changes on variation of ln β can be neglected. From the slope of a plot of ln λ against $(\ln \beta_0)^{-2}$, γ can be calculated. For the systems studied, such a plot is shown in Figure 6, and the fit results are given in Table 2. The data in Figure 6 show that there is a linear relation with good correlation coefficients (Table 2). The slopes yield an average surface free energy for formation of a nucleus in the β′ polymorph of about 3.4–3.9 mJ/m^{-2}, independent of the HP fraction. This value can be used to calculate the nucleation rate for modeling the crystallization kinetics. The real value of the surface free energy of a nucleus would be higher because nucleation type in bulk fats is heterogeneous and Equation 10 is valid for homogeneous nucleation. From homogeneous nucleation rates in the a polymorph of emulsified 10% HP/SF, we determined a surface free energy of about 4.1 mJ·m^{-2} (6,7).

The only unknown parameter for calculating the nucleating rate as a function of time or supersaturation is α, which is defined as the fraction of the triglyceride molecule that should be in a suitable conformation for incorporation in the nucleus. However, α may also account for other delaying factors. From

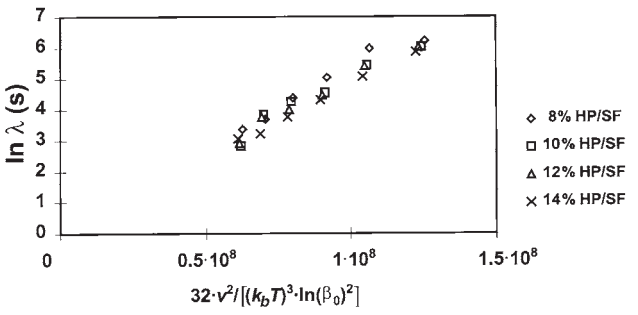

FIG. 6. Induction time λ as function of a supersaturation term to allow estimation of the surface free energy for nucleus formation.

TABLE 2
Estimation of the Surface Free Energy for Nucleation of HP/SF Mixtures[a]

HP/SF (%)	γ (mJ·m^{-2})	r^2 (–)
8	3.7 ± 0.2	0.978
10	3.6 ± 0.3	0.976
12	3.6 ± 0.2	0.988
14	3.6 ± 0.1	0.998

[a]Mixtures had various HP contents from the induction time for crystallization as a function of initial supersaturation. The induction time equals λ (*cf.* Eq. 7); *r* is the correlation coefficient. For abbreviations see Table 1.

the modeling of nucleation kinetics in emulsified fats, we calculated $\alpha \approx 1$ when nucleation was assumed to occur in the α polymorph (6,7). For heterogeneous nucleation in the β′ polymorph, α is expected to be smaller than 1 because once a molecule is partially incorporated in the closer packing of the β′ polymorph, the rest of the molecule will be forced to do also. Calculation of the crystallization curves showed that an α value of 0.8 resulted in an average final crystal radius of about 0.2 μm. This corresponds to a plate-shaped crystal with a length of 1.1 μm when it is assumed that it has the same volume as the spherical crystal and the length/width/thickness ratio is 10:2:1. This crystal length was about the size of primary structures that could be observed on polarized micrographs of samples crystallized at high supersaturation.

Because the nucleation rate and supersaturation are known as functions of time, it is possible to calculate the crystal growth rate R_c as a function of time or supersaturation. This was achieved by calculating, for every time step Δt, (i) the number of nuclei $J \cdot \Delta t$ produced, and (ii) by how much the crystals had to grow ($R_c \cdot \Delta t$) to yield the fraction crystallized given by Equation 8. After each time step, the nucleation rate corresponding to the new supersaturation was calculated, and the procedure was repeated. So, after each time step, a new crystal size interval was created. The growth rate at each time step was calculated by using a root-solving procedure.

It is assumed that the crystals are spherical. In reality, the crystals are platelets, having several growing faces, each having its own growth rate. The ratio of growth rates of the various faces equals the ratio of the crystal dimensions perpendicular to the faces. We suppose the crystals to be parallelepipeds, having three pairs of growing faces, *x*, *y*, and *z*, with linear growth rates R_x, R_y, and R_z, respectively. Furthermore, $R_x/R_y = a$ and $R_x/R_z = b$. The volume of the crystal in time can then be expressed as function of one growth rate and is given by $(a \cdot b)^{-1} \cdot R_x^{\,3} \cdot t^3$. If the ratio of the growth rates of the various faces will remain constant, the volume of a crystal and thereby the crystallization curves can be fitted by using only one crystal growth rate.

Because the modified Gompertz equation is unsuitable to fit the part of the crystallization curve between $t = 0$ and $t = \lambda$ (because the solid fat fraction could not be determined with sufficient accuracy), the growth rate in this time interval was calculated from the Avrami equation (16,17). The Avrami equation gives the solid fraction a function of time for constant *J* and R_c. Both parameters are constant for a constant supersaturation.

This will be approximately true between $t = 0$ and $t = \lambda$, and thus the Avrami equation can be used to calculate the initial R_c, because the nucleation rate J is known. We calculated the time after which 0.5% solids would be present, from Equation 8, and substituted this time in the Avrami equation. For spherical crystals that remain separate, the Avrami equation is:

$$s(t) = \frac{1}{3}\pi \cdot R_c^3 \cdot J \cdot t^4 \qquad [11]$$

After crystallization of 0.5% HP in a 10% HP/SF mixture, the supersaturation ratio is about 95% of its initial value. We neglected the effect of this decrease on the nucleation rate. At $t > \lambda$, the Gompertz equation was used to describe the amount of solid fat.

Figure 7 shows the fitted growth rates as a function of supersaturation for 12% HP/SF mixtures during crystallization at various initial supersaturations. These growth curves coincide for $\alpha = 0.8$ and $\gamma = 3.8$ mJ·m^{-2}, while for higher values of γ, the growth curves strongly deviate from each other.

The growth rate curves show some irregularities at the beginning of the crystallization process, i.e., at the right-hand side of the growth rate curves. This may be due to the change from the Avrami equation to the modified Gompertz equation at $t = \lambda$. Because the rates of increase of the solid fraction at a solids percentage of 0.50% differ for both equations, the calculated growth rate curve cannot be continuous at that point. Figure 7 shows that, for $\ln \beta > 1$, $\log R_c$ is linear with $\ln \beta$, and the growth rate curves can be described by a relation of the following form:

$$\ln R_c = \ln A_g + b_g \cdot \ln \beta \quad \text{or} \quad R_c = A_g \cdot \beta^{b_g} \qquad [12]$$

This type of equation is not equivalent to any of the theoretical growth rate equations given previously. We will come back to this point later.

Because now a function is known that empirically describes the growth rate as function of supersaturation, the crystallization curves can be fitted by varying only A_g and b_g for a given α and γ. Only the last part of the crystallization curve, corresponding to supersaturations below 0.8, cannot be fitted easily. There are two main advantages of using Equation 12: only two parameters are needed to describe the growth rate as function of supersaturation, and there is no discontinuity when going from the Avrami equation to the modified Gompertz equation.

The measured data were fitted to Equation 12 by minimizing the sum of the squares of the differences between the fitted and the measured fractions solid fat. Figure 8 shows the fitted lines. There are some small differences compared to the fits obtained with the Gompertz equation (Fig. 5).

The fit coefficients A_g and b_g from Equation 12 are compiled in Table 3 and show that, for supersaturations below 2.75, the slope b_g equals about 1.5. For supersaturations of 2.75 and higher, the slope decreases to a value of about 1.3. The same slopes were determined for mixtures containing various fractions of HP. The step change of b_g between $\ln \beta$ 2.50 and 2.75 is probably related to the morphology of the crystal structures. Polarized microscopic observations showed that spherulitic structures were formed for supersaturations below 2.75. At higher supersaturations, the polarized micrographs showed small structures with a typical size of 1 μm that were evenly distributed over space.

As mentioned, it was not possible to fit the crystallization curves by using one of the theoretical growth rate equations. Possible explanations for this observation are: (i) The common growth models are only suited for mixtures that are slightly supersaturated, say $\ln \beta$ of about 0.01 to 1. At higher supersaturations, their applicability is limited because: heat of crystal-

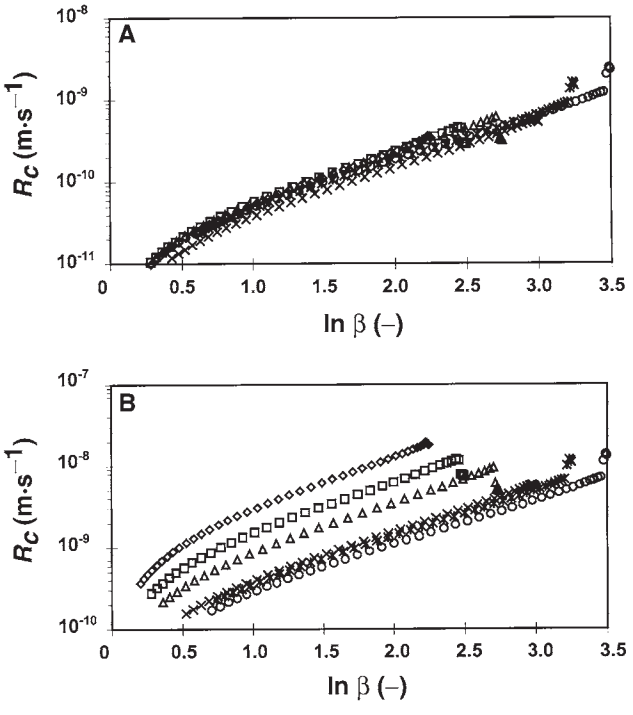

FIG. 7. Growth rate (R_c) curves calculated from crystallization curves of 12% HP/SF mixtures for various initial supersaturations. ln β_0: ◇, 2.25; □, 2.50; △, 2.75; × 3.00; *, 3.25; ○, 3.50. Nucleation parameters: α = 0.8; (A): γ = 3.8 mJ·m^{-2}; (B): γ = 5.0 mJ·m^{-2}. See Figures 1 and 2 for abbreviations.

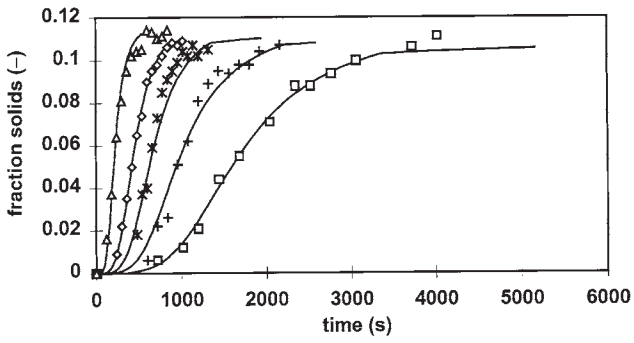

FIG. 8. Measured and fitted crystallization curves of 12% HP/SF mixtures crystallized at various initial supersaturations. The fits were obtained from growth rate (Eq. 11). Initial supersaturation: □, 2.25; +, 2.50; *, 2.75; ◇, 3.00; △, 3.25. See Figures 1 and 2 for abbreviations.

TABLE 3
Coefficients A_g and b_g from Growth Rate[a]

ln β_0 (–)	A_g (m·s^{-1})	b_g (–)
2.25	$1.4 \cdot 10^{-11}$	1.50
2.50	$1.1 \cdot 10^{-11}$	1.50
2.75	$1.39 \cdot 10^{-11}$	1.31
3.00	$1.24 \cdot 10^{-11}$	1.31
3.25	$1.78 \cdot 10^{-11}$	1.31
3.50	$1.80 \cdot 10^{-11}$	1.31

[a]Values obtained from a fit of isothermal crystallization curves of 12% HP/SF mixture at various initial supersaturation. See Table 1 for abbreviation.

lization has to be removed and molecules may not be able to diffuse fast enough to reach the crystal surface. Both phenomena can result in an effectively lower supersaturation at the solid–liquid interface than is calculated on the basis of the amount of crystallized material. Assuming a heat diffusion coefficient D^* of 10^{-7} m^2/s, the radius of p-NMR tube R = 4 mm, and the Fourier number Fo(cylinder) = $D^* \cdot t_{0.5}/R^2$ = 0.2 yields a characteristic time $t_{0.5}$ of 32 s, during which the amount of heat is halved. A maximum crystallization rate of $6 \cdot 10^{-4}$ s^{-1} (μ in Eq. 7; 12% HP/SF, ln β_0 = 3.50) corresponds to a temperature increase rate of 0.027 K/s, assuming a specific heat capacity of 4 kJ·kg^{-1}K^{-1} and no heat loss. In $t_{0.5}$, the temperature increase would be about 0.9 K, which will certainly affect the real supersaturation. Also, the diffusion length of a triglyceride molecule at $D^* = 10^{-11}$ m^2/s is about $3 \cdot 10^{-6}$ m for $t_{0.5,d}$ = 1 s. This distance is much larger than the displacement of the solid–liquid interface in 1 s, which is at most 10 nm. Hence, the crystallization rate would not be diffusion-limited.

(ii) Because HP consists of various triglycerides, the supersaturation, which determines the magnitude of the nucleation rate, is a rather ill-defined term. The supersaturation is calculated for the mean thermodynamic bulk properties of HP/SF mixtures, while during crystallization, some fractionation of triglycerides may occur.

(ii) Due to the variety of triglycerides, crystal defects will form that can influence the incorporation of other triglycerides at the crystal surface. The description of the crystal growth kinetics is even more hampered due to the competition between various not perfectly matching triglyceride molecules.

(iv) The anisometric shape of the triglyceride molecule and of the crystal will greatly hamper the microscopic description of the incorporation process of a triglyceride molecule. It is not unlikely that the activity coefficients depend on the supersaturation in a different way for each crystal face.

(v) It is assumed that the nucleation rate can be described by the classical nucleation rate equation, although it is by no means sure that it is allowable. For instance, no direct account is made for the occurrence of secondary nucleation. However, its effect may perhaps be incorporated as an apparent surface free energy.

(vi) Aggregation and sintering of crystals will lead to a decrease in the effective crystal surface and therefore to a lower crystallization rate. This will become more pronounced if strong clustering of crystals to compact aggregates or thickened crystal strands occurs, i.e, in later stages of the crystallization process.

Aggregation and gelation times. Although, as discussed above, there are many uncertainties in describing the crystal growth rate as a function of supersaturation, it may provide important information about the crystal-size distribution as a function of time, which can be used to estimate aggregation or gel times. Fat crystals aggregate due to van der Waals forces as soon as the crystals become large enough to overcome thermal energy. The aggregation time is the time needed to halve the number of particles, and for rapid diffusion-limited aggregation of spherical particles is given by (17):

$$t_{0.5} = \frac{3 \cdot \eta}{4 \cdot k_b T \cdot c_0} = \frac{\pi \cdot \eta \cdot a^3}{k_b T \cdot \phi} \qquad [13]$$

where η is the viscosity of the continuous phase, c_0 the number concentration crystals, a the crystal radius, and ϕ the volume fraction solid fat. At a low volume fraction of crystallized fat, the fat crystal aggregates have a fractal structure with a fractal dimensionality D of about 1.7 (6,19). Ongoing aggregation then will lead to gelation. The gel time for fractal aggregation is given by (20):

$$t_{gel} = z^{D-1} \cdot \left(1 - \frac{6D}{2D+3} + \frac{3D}{D+6}\right) \cdot \frac{\pi \cdot \eta \cdot a^3}{k_b T} \cdot \phi^{\frac{3}{D-3}} \qquad [14]$$

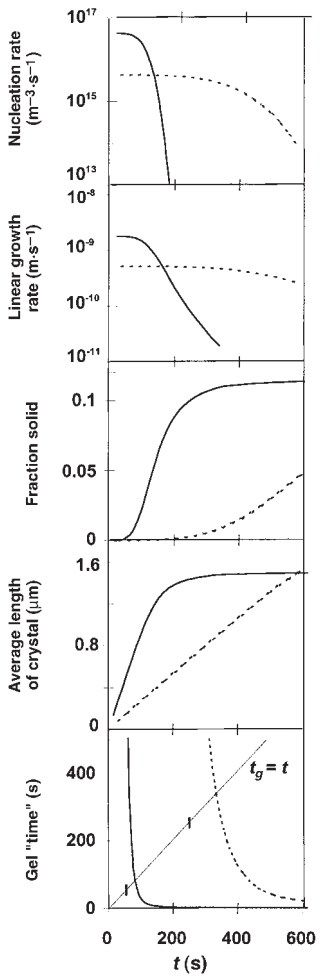

FIG. 9. Values of various crystallization parameters as a function of time (t) after cooling of 12% HP/SF systems at initial (ln β_0) supersaturations of 2.75 (dotted line) and 3.50 (solid line). Results are calculated from experimental data on nucleation and growth. See Figures 1 and 2 for abbreviations.

where z is a constant depending on the fractal dimensionality ($z = 0.884$ for $D = 1.7$). Because the average crystal size and the volume fraction of solid fat are known as function of time, the time scales of aggregation and gelation can be evaluated as function of crystallization time. Figure 9 compiles various crystallization parameters as function of time. It shows that gelation already occurs early in the crystallization process. Short time scales for aggregation and gelation were indeed observed from steady shear viscosity measurements during the aggregation of fat crystals in low-volume fraction solids mixtures and dynamic rheological measurements on crystallizing mixtures (6,21). Gelation already occurs at a solid fat fraction of 0.01 or less, implying that a continuous network is formed long before crystallization is complete. The order of magnitude of the time scale for gelation agrees well with gel times ranging from 40 to 330 s, as determined by dynamical rheological measurements of 12% HP/SF mixtures at initial supersaturations of 3.50 and 2.75, respectively (6). The structure of the fat crystal aggregates and the mechanical properties of the fat crystal networks will be discussed elsewhere.

ACKNOWLEDGMENTS

We thank Dr. Richard Leloux and Prof. Henk Schenk from the University of Amsterdam for allowing us to use the time-resolved X-ray diffraction equipment. DSC experiments were carried out by Jerry van Manen from TNO-Nutrition, Zeist. Valuable discussions with Dr. Woulter L.J. Meeussen are gratefully acknowledged.

REFERENCES

1. van den Tempel, M., Mechanical Properties of Plastic-Disperse Systems at Very Small Deformations, *J. Colloid. Sci 16*:284–296 (1961).
2. Walstra, P., T. van Vliet, and W. Kloek. Crystallization and Rheological Properties of Milk Fat, in *Lipids*, 2nd edn., edited by P.F. Fox, Chapman & Hall, London, 1995, Vol. 2, pp. 179–211.
3. Walstra, P., and R. Jennes, *Dairy Chemistry and Physics*, Wiley, New York (1984).
4. Hannewijk, J., Kristallisatie Van Vetten I, *Chem. Weekblad 60*:309–316 (1964).
5. Wesdorp, L.H., Liquid—Multiple Solid-Phase Equilibria in Fats—Theory and Experiments, Ph.D. Thesis, Technical University of Delft, The Netherlands, 1990.
6. Kloek, W., Mechanical Properties of Fats in Relation to Their Crystallization, Ph.D. Thesis, Wageningen Agricultural University, The Netherlands, 1998, pp. 24–52.
7. Kloek, W., P. Walstra, and T. van Vliet, Nucleation Kinetics of Emulsified Triglyceride Mixtures, *J. Am. Oil Chem. Soc. 77*, in press.
8. Skoda, W., and M. van den. Tempel, Growth Kinetics of Triglyceride Crystals, *J. Crystal Growth 1*:207–217 (1967).
9. Garside, J., Industrial Crystallization from Solutions, *Chem. Engineering Sci. 40*:3–26 (1985).
10. Garside, J., General Principles of Crystallization, in *Food Structure and Behaviour*, edited by J.M.V. Blanshard and P. Lillford, Academic Press, London, 1987, pp. 35–49.
11. Boistelle, R., Fundamentals of Nucleation and Crystal Growth, in *Crystallization and Polymorphism of Fats and Fatty Acids*, edited by N. Garti and K. Sato, Marcel Dekker, New York, 1988, pp. 189–226.
12. Burton, W.K., N. Cabrera, and F.F. Frank, The Growth of Crystals and the Equilibrium Structure of Their Surfaces, *Philos. Trans. R. Soc. A243*:299–358 (1951).
13. Heertje, I., and M. Pâques, Advances in Electron Microscopy, in *New Physico-Chemical Techniques for the Characterization of Complex Food Systems*, edited by E. Dickinson, Chapman and Hall, London, 1995, pp. 1–52.
14. Malkin, T., The Polymorphism of Glycerides, *Prog. Chem Fats Lipids 2*:1–50 (1954).
15. Zwietering, M.H., I. Jongenburger, F.M. Rombouts, and K. vant Riet, Modeling of the Bacterial Growth, *Appl. Environ. Microbiol. 56*:1875–1881 (1990).
16. Avrami, M., Kinetics of Phase Change. I. General Theory, *J. Chem. Phys. 7*:1103–1112 (1939).
17. Avrami, M., Kinetics of Phase Change. II. Transformations—Time Relations for Random Distribution of Nuclei, *J. Chem. Phys. 8*:212–224 (1939).
18. von Smoluchowski, M., Versuch Einer Mathematischen Theorie der Kogulationskinetik Kolloider Lösungen, *Z. Physik. Chem. 92*:129–168 (1917).
19. Vreeker, R., L.L. Hoekstra, D.C. den Boer, and W.G.M. Agterof, The Fractal Nature of Fat Crystal Networks, *Colloids Surf. 65*:185–189 (1992).
20. Bremer, L.G.B., Fractal Aggregation in Relation to Formation and Properties of Particle Gels, Ph.D. Thesis, Wageningen Agricultural University, The Netherlands (1992).
21. Kloek, W., P. Walstra, and T. van Vliet, Mechanical Properties of Fat Crystal Networks, in *Food, Gels and Polymers*, edited by F. Dickinson and B. Bergenstahl, Royal Society of Chemistry, London, 1997, pp. 168–181.

[Received April 29, 1999; accepted December 2, 1999]